IIETA International Information and Engineering Technology Association
Advancing the World of Information and Engineering

Mathematical Modelling of Engineering Problems
Vol. 10, No. 3, June, 2023, pp. 968-978
Journal homepage: http://iieta.org/journals/mmep

Evaluating the Effects of Air Cooling on Photovoltaic Module Performance in Hot Climates: A Comprehensive Numerical and Experimental Investigation

Ahmed J. Hamad[1*], Fawizea M. Hussein[1], Ali Lateef Tarish[2]

[1] Mechanical Power Engineering Department, Engineering Technical College, Middle Technical University, Baghdad 10090, Iraq
[2] Department of Thermal Mechanical, Engineering Technical College/Basra, Southern Technical University, Basra, 61002, Iraq

Corresponding Author Email: ahmed.elhamad@mtu.edu.iq

https://doi.org/10.18280/mmep.100330

Received: 5 January 2023
Accepted: 13 March 2023

Keywords:
PV module temperature, electrical efficiency, output power, air-cooling, simulation model, numerical solution

ABSTRACT

The performance of solar photovoltaic (PV) modules is significantly impacted by heat accumulation within the module materials, resulting from solar irradiance. This heat accumulation leads to increased module temperatures and decreased output power. Consequently, enhancing the cooling performance of PV modules can improve their output power, electrical efficiency, and extend their operational lifespan. In this study, the influence of air cooling on solar PV module performance under hot climatic conditions was investigated experimentally and numerically for various ambient temperatures (35, 40, 45℃) and irradiance levels (G: 800, 900, 1000 W) at different air flowrates. A numerical investigation was conducted using a turbulent flow simulation model, solved with COMSOL Multiphysics 5.4 software. Results demonstrated a considerable reduction in PV module temperature as the cooling air flowrate increased under diverse testing conditions. Module temperature increments of approximately 1.8% and 4% were observed for G=900 W and 1000 W, respectively, when compared to G=800 W. The output power of PV modules incorporating air cooling exhibited enhancements of roughly 8.2%, 7%, and 5.4% for irradiances of 800, 900, and 1000 W, respectively, compared to those without cooling. Furthermore, the electrical efficiency of PV modules with air cooling improved by approximately 4%, 4.4%, and 5% for irradiances of 800, 900, and 1000 W, respectively, in comparison to those lacking cooling mechanisms.

1. INTRODUCTION

The efficiency of solar photovoltaic (PV) panels is heavily influenced by environmental conditions, particularly ambient temperature. In hot climatic zones, the accumulation of solar radiation energy within the PV panel can lead to a significant decrease in efficiency and output power, with module temperatures potentially exceeding 65℃ [1-4]. It is estimated that only about 20% of solar irradiance is converted into electric power, while the remaining 80% is converted into heat [5]. Consequently, the development of improved cooling techniques for PV panels can minimize panel temperature and enhance overall performance. The power output of PV panels is primarily dependent on their operating temperature, with a 1℃ rise in temperature leading to a reduction in module efficiency of approximately 0.03-0.5% [6-9]. Numerous studies have focused on the temperature-dependent efficiency of PV modules and its effect on output power.

An increased understanding of the operational principles of photovoltaic panels has led to a rapid improvement in the efficiencies of power conversion for PV panels [10-13]. Several researchers have investigated the effect of outdoor conditions on PV module efficiency in hot climate regions, examining various environmental conditions both experimentally and numerically to demonstrate their influence on PV module operation. It has been observed that the loss in open circuit voltage and output power of the PV module is -0.104/℃ and -1.3/℃, respectively, while the efficiency drop is approximately 9.62% compared to standard conditions [14-16].

Various cooling methods have been employed to enhance PV module efficiency, including passive cooling using fins, active cooling based on air and water cooling, cooling with phase change materials (PCM), and cooling using PCM with porous metals or nanoparticles [17-23]. Research has shown that when cooling systems are used, PV module output power is improved. Several studies have investigated passive cooling methods using fins installed on the backside of the PV panel to enhance module performance. Aluminum fins have been applied to the back panel of solar cells with various configurations to reduce PV module operating temperature, with different fin parameters such as length and sequences analyzed to assess module efficiency and power [24-28].

Water-cooling systems have also been explored by numerous researchers as a means to minimize PV module temperature and improve performance [29-32]. Different designs and technologies of water-cooling systems have been utilized to enhance the cooling effect for conventional and concentrated PV panel systems. The output power of water-cooled concentrated PV systems has been shown to improve by approximately 24.4% compared to systems without cooling. Additionally, the total efficiency for PV module systems with water cooling has improved in the range of 17-18.04% compared to systems without cooling mechanisms.

A review of the literature reveals that most researchers have conducted experimental and numerical analyses to evaluate the cooling performance of solar PV modules using various cooling techniques. However, the research area of investigating the air-cooling performance of solar PV module systems under hot environmental conditions remains relatively unexplored. Therefore, the present study presents an experimental and numerical analysis to investigate the air-cooling effect on PV module performance under the extremely hot climatic conditions of Baghdad city (latitude 33 19′ N and longitude 44 25′ E). The numerical analysis is based on a turbulent flow simulation model and is solved using COMSOL Multiphysics 5.4 software. Various PV module performance parameters are investigated in this work and validated with data reported in the literature under similar operating conditions.

2. MATERIALS AND METHODS

2.1 PV module system experimental setup

The specifications of solar PV module used with the air-cooling system considered in the present investigation is illustrated in the Table 1. This system is consisting of a Polycrystalline solar module of model Orex: AR- M300W with dimensions (1955×990×40 mm) attached to air cooling channel as shown in Figure 1. The PV module consists of three layers namely, glass sheet at the outer surface subjected to the solar radiation, Polycrystalline silicon cells layer, and Tedlar layer at the back of the PV module. Air cooling channel represents a rectangular duct of dimensions (1960×995×10 mm) fabricated from 1 mm thickness Aluminum sheets and thermally insulated by glass wool (k=0.038 W/m.℃) from the bottom and sides for minimizing heat loss to the surrounding as shown in Figure 2. Thermophysical properties of the PV module layers under study are illustrated in Table 2. The solar PV module was installed on a supporting stand inclined with variable angles of 20 to 45 degree with the horizontal and oriented to west south direction to facing the solar radiation. Air at ambient temperature is forced to flow into a cooling duct for cooling the solar PV module using a variable power centrifugal fan of model LMN249HVT, 60 W capacity and flowrate 12.8 m^3/min. The air fan with an electrical heater of power 3000 W was installed at air duct inlet to supply the cooling air with specified flowrate and temperature considered in the three test cases as shown in Figure 2. The velocity of air flowing through the air-cooling duct was measured using a digital Anemometer of model GM8901. Three K-type thermocouples of the range -200 to 1250℃ were used to measure the ambient, duct inlet and outlet temperatures, and five thermocouples located at different positions on the PV module back surface were used to measure the solar panel surface temperature. Data logger of model BTM-4208SD and accuracy ±0.2℃ was utilized to record and display the temperatures, while the solar irradiance was recorded using irradiance meter of model SEAWARD-R200 with a measuring range of 100–1250 W/m^2, and accuracy of ±5 W/m^2. All measuring devices are calibrated before starting the experimental tests.

2.2 Experimental methodology

The experimental work was conducted in July and August 2022 under Iraq-Baghdad city (Latitude 33 19′ N and longitude 44 25′ E) climatic conditions. Three testing cases are experimentally investigated based on ambient temperatures 35, 40 and 45℃, at three irradiances 800, 900, and 1,000 W/m^2 as illustrated in the Table 3. These testing conditions are selected to evaluate the PV module performance before and at peak hot hours of Baghdad city in the summer during day hours 10.00 am to 14.00 as shown in Figure 5. At first testing case, the inlet cooling air temperature was specified at 35℃, and the PV module cooling performance was investigated at solar irradiances 800, 900, and 1000 W/m^2 with inlet air flowrates 0.063, 0.084, 0.104, 0.125 (kg/s) using air fan supplied with electric heater. This step was repeated at inlet ambient air temperatures 40 and 45℃ which are considered extreme hot temperatures, and all measurements of air temperature, solar PV module surface temperature, air velocity and solar irradiance are monitored and recorded. The experimental data are employed to evaluate the performance of the solar PV module including output power, electrical efficiency, PV module surface temperature and heat transfer characteristics under different operating conditions with and without using air cooling.

Table 1. Specifications of the solar polycrystalline module [12]

Model	Orex: AR- M300W
Rated maximum power	300W
Tolerance (%)	0 ~ +3%
Voltage at maximum power (V_{mp})	36V
Current at maximum power (I_{mp})	8.33A
Open circuit voltage (V_{oc})	42.8V
Short circuit current (I_{sc})	9A
Temperature coefficient of Pmax	-0.4% /℃
Dimension	(1955 x 990 x 40 mm)

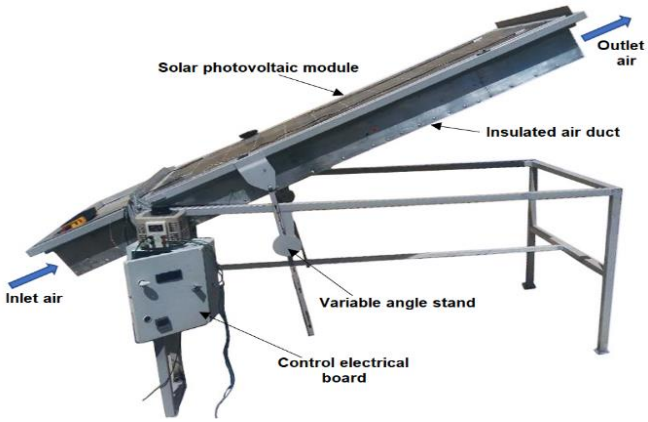

Figure 1. PV Module system experimental setup

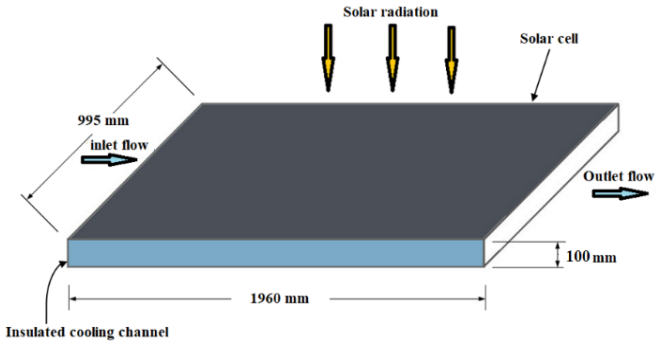

Figure 2. Air cooling duct of the PV module system

Table 2. Thermophysical properties of the solar polycrystalline PV module system [33]

Layer	Thickness (mm)	Density (kg/m^3)	Heat capacity (J/kg.°C)	Thermal conductivity (W/m.°C)
Glass layer	3.0	3000	500	1.8
Silicon cells layer	0.3	2330	677	148
Tedlar layer	0.5	1200	1250	0.2
Aluminum sheet	1	2719	871	202.4

Table 3. Testing cases considered in the experimental work

Case study	T_{air} (°C)	Air flowrate (kg/s)	Solar radiation (W/m^2)
1	35	0.063, 0.084, 0.104, 0.125	800, 900, 1000
2	40	0.063, 0.084, 0.104, 0.125	800, 900, 1000
3	45	0.063, 0.084, 0.104, 0.125	800, 900, 1000

2.3 Mathematical modeling

The proposed solar PV module and air-cooling system considered in the present numerical and experimental investigation is simulated using a mathematical model based on continuity, momentum, and energy conservation principles. The modeling of heat transfer between the PV module back sheet and the cooling air flowing in the air channel was based on forced convection and turbulent flow of Reynold's number (*Re*) in the range of 6000-12000. The simulation model including governing equations and turbulence model (k-ε) was solved numerically using COMSOL Multiphysics -5.4 software.

2.3.1 Assumptions

The simulation model of the solar PV module and cooling system is formulated based on the following assumptions:

1. Airflow in the cooling duct attached to the PV module back surface was assumed three-dimensional and turbulent flow.
2. Unsteady and incompressible airflow.
3. Solar PV panel is assumed at constant thermal properties and subjected to direct solar radiation.
4. The bottom and side surfaces of the air channel are well insulated; therefore, the channel surface is considered adiabatic except for the upper surface attached to the PV panel.
5. A perfect thermal contact is assumed between layers of the solar PV panel.

2.3.2 Governing equations

The governing equations can be expressed in conservation form as follows [29, 33].

Continuity Equation:

$$\frac{\partial u}{\partial x}+\frac{\partial u}{\partial y}+\frac{\partial u}{\partial z}=0 \tag{1}$$

Momentum Equation:

$$\frac{\partial \rho u}{\partial t}+\nabla.(\rho uV)=-\frac{\partial p}{\partial x}+\mu\left(\frac{\partial^2 u}{\partial x^2}+\frac{\partial^2 u}{\partial y^2}+\frac{\partial^2 u}{\partial z^2}\right)+\rho f x \tag{2}$$

$$\frac{\partial \rho v}{\partial t}+\nabla.(\rho vV)=-\frac{\partial p}{\partial y}+\mu\left(\frac{\partial^2 v}{\partial x^2}+\frac{\partial^2 v}{\partial y^2}+\frac{\partial^2 v}{\partial z^2}\right)+\rho f y \tag{3}$$

$$\frac{\partial \rho w}{\partial t}+\nabla.(\rho wV)=-\frac{\partial p}{\partial z}+\mu\left(\frac{\partial^2 w}{\partial x^2}+\frac{\partial^2 w}{\partial y^2}+\frac{\partial^2 w}{\partial z^2}\right)+\rho f z \tag{4}$$

where, V and u, v, w, are flow vector velocity and velocity components in (x, y, z) space, t is time, ρ is air density and f is body force per unit mass, and μ is absolute viscosity.

Energy Equation:

For solar PV panel and air flow:

$$\frac{\partial(\rho CpT)}{\partial t}+\nabla.(\rho CpVT)=\nabla.(k\nabla T)+gV+\rho T\frac{DCp}{Dt} \tag{5}$$

$$\frac{\partial^2 T}{\partial x^2}+\frac{\partial^2 T}{\partial y^2}+\frac{\partial^2 T}{\partial z^2}=\frac{\rho Cp}{k}\frac{\partial T}{\partial t} \tag{6}$$

where, g is represents the rate of heat source within the material per unit volume, and k is thermal conductivity.

The turbulence model was mathematically formulated using standard (k-ε) model because it is a reliable, less computational time and with reasonable accuracy. The standard (k-ε) model falls within the two-equation models in which the solution of two separate transport equations allows the turbulent velocity and length scales to be independently determined. This model is based on transport equations for the turbulence kinetic energy (k) and dissipation rate (ε).

The turbulence kinetic energy (k) is obtained from the transport equation:

$$\frac{\partial}{\partial t}(\rho k)+\frac{\partial}{\partial x_i}(\rho k u_i)=\frac{\partial}{\partial x_j}\left[\left(\mu+\frac{\mu_t}{\sigma_k}\right)\frac{\partial k}{\partial x_j}\right]+G_k+G_b-\rho\epsilon-Y_M+S_k \tag{7}$$

The rate of dissipation (ε), is obtained from the transport equation:

$$\frac{\partial}{\partial t}(\rho\varepsilon)+\frac{\partial}{\partial x_i}(\rho\varepsilon u_i)=\frac{\partial}{\partial x_j}\left[\left(\mu+\frac{\mu_t}{\sigma_\varepsilon}\right)\frac{\partial \varepsilon}{\partial x_j}\right]+C_{1\varepsilon}\frac{\varepsilon}{k}(G_k+C_{3\varepsilon}G_b)-C_{2\varepsilon}\rho\frac{\varepsilon^2}{k}+S_\varepsilon \tag{8}$$

S_k on the right-hand side of the Eq. (7), and S_ε in Eq. (8) can be specified as a constant or user-defined source term. These terms S_k and S_ε are considered zero in the current analysis.

The turbulent viscosity μ_t is expressed by:

$$\mu_t=\rho C_\mu\frac{k^2}{\varepsilon} \tag{9}$$

The mean velocity gradients G_k for the turbulence kinetic energy generation is defined as:

$$G_k=-\rho\overline{\acute{u}_i\acute{u}_j}\frac{\partial u_j}{\partial x_i} \tag{10}$$

The Reynolds stresses ($-\rho\overline{\acute{u}_i\acute{u}_j}$) can be defined by Eq. (11):

$$-\rho\overline{\acute{u}_i\acute{u}_j} = \mu_t\left(\frac{\partial u_i}{\partial x_j}+\frac{\partial u_j}{\partial x_i}\right)-\frac{2}{3}\left(\rho k+\mu_t\frac{\partial u_k}{\partial x_k}\right)\delta_{ij} \quad (11)$$

where, $\acute{u}_i$ *and* $\acute{u}_j$ are the fluctuating velocity components (i=1, 2, 3).

The turbulence kinetic energy generation due to buoyancy G_b can be defined by:

$$G_b = \beta g_i \frac{\mu_t}{Pr_t}\frac{\partial T}{\partial x_i} \quad (12)$$

where, Pr_t is the turbulent prandtl number for energy (Pr_t=0.85), g_i is the component of the gravitational vector and β is the coefficient of thermal expansion.

YM: represents the contribution of the fluctuating dilatation in compressible turbulence to the overall dissipation rate and defined by:

$$Y_M = 2\rho\varepsilon M_t^2 \quad (13)$$

The turbulent Mach number is defined as:

$$M_t = \sqrt{\frac{k}{a^2}} \quad (14)$$

$$a = \sqrt{\gamma R\, T} \quad (15)$$

σ_k and σ_ε are the turbulent Prandtl numbers for k and ε, and the model constants have the following default values [34]:

$C_{1\varepsilon}$=1.44, $C_{2\varepsilon}$=1.92, $C_{3\varepsilon}$=1, $\sigma_k = 1$, σ_ε =1.3, C_μ=0.09

Reynold's number and Nusselt's number are presented in the Eq. (16) and Eq. (17) respectively.

$$Re=\frac{\rho v D_h}{\mu} \quad (16)$$

$$Nu=\frac{\alpha D_h}{k} \quad (17)$$

where, α is a convection heat transfer coefficient (W/m^2.℃), and D_h represents the hydraulic diameter of the air duct rectangular cross-sectional area, and can be expressed by:

$$D_h=\frac{4\,A_c}{p} \quad (18)$$

where, A_c and p are the cross-sectional area and perimeter of the air duct respectively.

2.3.3 Boundary conditions

Referring to the computational domain of the simulated PV module air cooling system shown in Figure 3, the boundary conditions of the cooling channel can be expressed as follows:

Cooling channel inlet: The air temperature, velocity and pressure are considered as, T=*Tin*, V=*Vin*, and p=p_{am}, where V represents air velocity vector with components in x, y, z directions.

Cooling channel outlet: At the air channel exit, a fully developed flow is considered, all the flow property gradient is assumed equal to zero, and p_{air}=p_{am}.

Solid boundary: The cooling channel (air duct) internal surfaces exposed to the airflow are considered at no-slip condition (V=0). The external bottom and side surfaces of the channel are insulated and considered adiabatic (∂q=0), while the channel upper surface attached to the PV panel is subjected to heat flux (q) of the solar radiation G(W/m^2), (q=G).

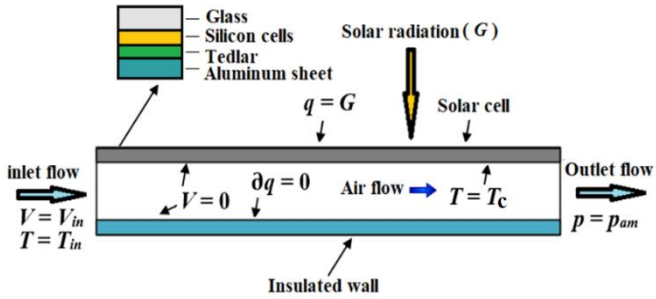

Figure 3. Boundary conditions of the computational domain

2.3.4 Meshing and grid independence verification

To verify the appropriate mesh size for the computational domain considered in the simulation model depicted in Figure 4, a grid dependency was examined based on PV module temperature (Tc) as a reference. The grid dependence test is necessary for optimizing the computation time and accuracy of COMOSL software's numerical solution. Three types of meshing; fine, finer, and extra fine are examined to investigate the appropriate mesh size for saving computational time with acceptable accuracy as indicated in Table 4. It was observed that there is no significant difference in the value of Tc between them, therefore a fine mesh with 84217 elements and 31316 refined grids near the walls was adopted to minimize the computation time in the present numerical solution.

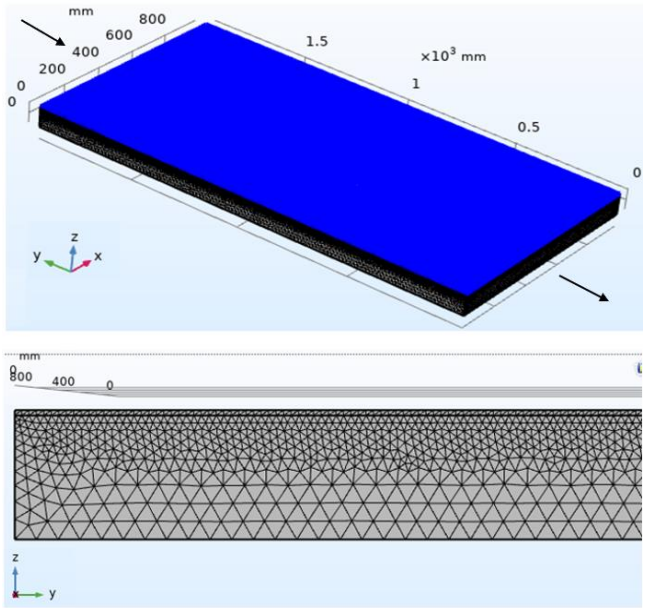

Figure 4. Computational domain and mesh of the PV module simulation model

Table 4. Grid independence verification based on PV module temperature (Tc)

Mesh type	Number of domain elements	Number of boundary elements	Tc (℃)
Fine	84217	31316	44.12
Finer	262097	89924	44.14
Extra fine	2066523	531324	44.18

2.4 PV module performance parameters

The performance parameters of the PV module including output power, electrical efficiency, and thermal efficiency are calculated based on the assumption of constant thermal properties for the PV module and subjected to a direct solar radiation as illustrated in Tables 2 and 3. The effect of the solar cell surface temperature on PV module electrical efficiency can be evaluated by the following equation [35, 36]:

$$\eta_{el} = \eta_{rf}\,[\,1 - \beta_{rf}(T_c - T_{rf}) + \gamma log_{10}\,G] \qquad (19)$$

where, the typical quantities η_{rf} and β_{rf} of PV module are given in the data sheet by module manufacturer, where the reference efficiency η_{rf}=15.6% and β_{rf}=0.4%.

T_c is the actual measured PV module surface temperature, and the standard cell temperature T_{rf}=25°C.

The solar radiation coefficient γ represents material property, γ=0.12 for monocrystalline silicon cell. The last term ($\gamma log_{10}\,G$) can be neglected and Eq. (19) reduced to:

$$\eta_{el} = \eta_{rf}\,[\,1 - \beta_{rf}(T_c - T_{rf})] \qquad (20)$$

The electrical efficiency of solar PV module can be expressed by [37, 38]:

$$\eta_{el} = \frac{P_c}{G\,A_c} \qquad (21)$$

where, G represents the solar irradiance (W/m^2), A_c is solar cell surface area (m^2) and P_c represents the solar cell maximum output power which is determined by Eq. (22):

$$P_c = I_{mp}\,V_{mp} \qquad (22)$$

where, I_{mp} and V_{mp} are the measured current (Ampere) and voltage (Volt) respectively at maximum output power of the solar PV module. The convection heat transfer coefficient (α) can be estimated experimentally by Eq. (23):

$$\alpha = \frac{G}{A_c\,(T_c - T_m)} \qquad (23)$$

where, T_c and T_m are the actual measured PV module surface and mean air temperatures respectively. The thermal efficiency of the solar PV module air cooling is given by Eq. (24):

$$\eta_{th} = \frac{m_{air}\,Cp\,(T_o - T_i)}{A_c\,G} \qquad (24)$$

3. RESULTS AND DISCUSSION

3.1 Experimental Results

To investigate the effect of air-cooling on solar PV module performance under hot climatic conditions, three testing cases are considered based on different ambient temperatures (35, 40, 45°C) and irradiances (800, 900, 1000 W) as illustrated in Table 3. The performance parameters of the solar cell were investigated at relatively high ambient temperature (45°C) to simulate the Baghdad city hot climatic conditions in the summer. The variations of average ambient temperature and solar radiation with day hours during the experimental testing period in July and August 2022 are shown in Figure 5. It can be observed that the higher ambient temperature and irradiance were at peak sunshine period during the day hours 12 to 14 where, T_{am}=45°C and G=1000 W under test conditions, as illustrated in this figure.

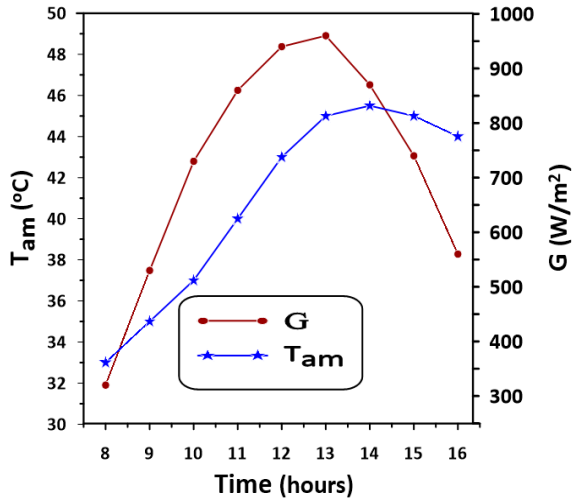

Figure 5. Average ambient temperature and solar irradiance variations with the day hours during the testing period

3.1.1 Effect of the cooling on PV module temperature

The variations of the solar PV panel temperature with air flowrate in the cooling channel at different irradiances and ambient temperatures are shown in Figure 6. A noticeable drop in the PV module temperature with cooling air flowrate increasing can be seen under different conditions. In addition, it can be observed an escalating rise in the module temperature with increase in the solar radiation and ambient temperature. This increasing in the module temperature is attributed to the heat energy accumulation within PV module surface due to incidence of the solar radiation on cell surface. Test conditions at G=1000 W and T_{am}=45°C have revealed a maximum temperature of about Tc=65°C at relatively minimum air flowrate of 0.063 kg/s. While the minimum module temperature was 47°C at G=800 W and T_{am}=35°C.

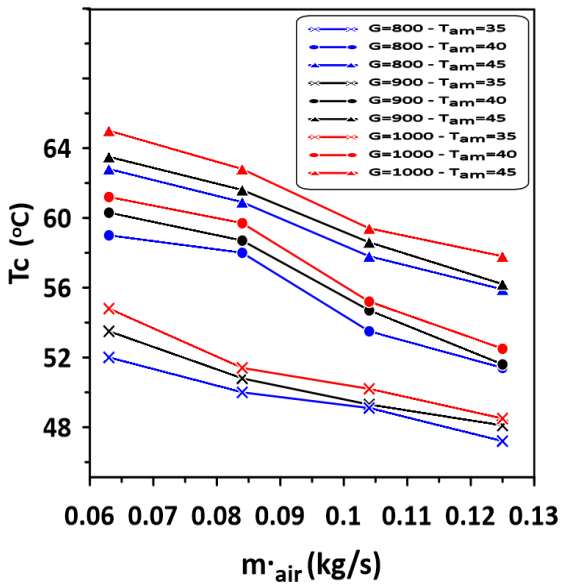

Figure 6. Variation of *Tc* with air flowrate at different irradiances and ambient temperatures

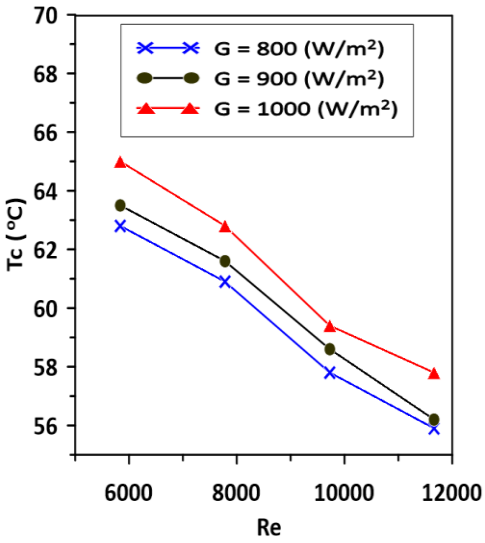

Figure 7. Variation of *Tc* with *Re* of the air flow at different irradiances and T_{am}=45℃

Figure 7 shows the variation of the solar cell surface temperature with *Re* of the cooling air flow at different irradiances 800, 900, 1000 W, and T_{am}=45℃. It can be seen a continuous reduction in PV module temperature with *Re* increasing as a result of air-cooling effect and forced convection heat transfer between the panel surface and air. Comparison of the results at Reynold's number in the range of 5837 - 11663 reflected an increase in the module temperature by about 1.8% and 4% for *G*=900 W and 1000 W respectively compared with that for *G*=800 W. The variations of *Nu* with Reynold's number of the cooling air flow at different irradiances and T_{am}=45℃ are shown in Figure 8. A noticeable rise in *Nu* with *Re* increasing can be observed as a result of enhancement in heat exchange between the module surface of relatively higher temperature and flowing air in the cooling channel. Nusselt's number for *G*=900 W and 1000 W were greater by about 15.4% and 24.7% respectively compared with that for *G*=800 W.

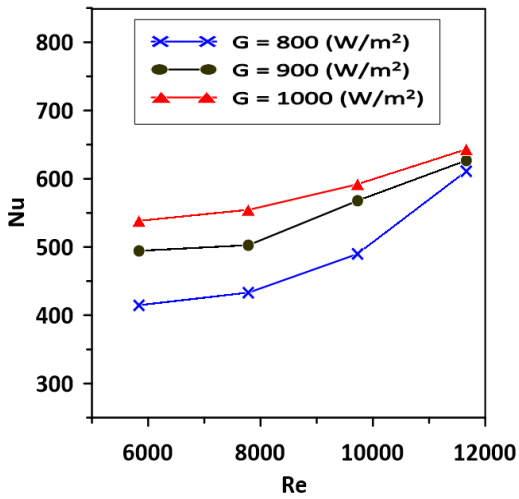

Figure 8. Variation of *Nu* with *Re* at different irradiances and T_{am}=45℃

3.1.2 Effect of the cooling on PV module performance

The performance parameters of the PV module and air-cooling system including output power, electrical efficiency, and thermal efficiency at various testing conditions are investigated. Variation of the module output electrical power with air flowrate without and with cooling at different irradiances 800, 900, 1000 W, and T_{am}=45℃ is shown in Figure 9. It can be observed a noticeable rise in PV module output power with air flowrate increasing due to the cooling effect on solar panel surface. Maximum output power was 261 W for *G*=1000 W at flowrate 0.125 kg/s, while the minimum output power was 196 W for *G*=800 W at flowrate 0.063 kg/s. Comparison of the output power results for PV module with air cooling at various irradiances shows an improvement in the power by about 8.2%, 7% and 5.4% for irradiances 800, 900 and 1000 W respectively compared to that without cooling. Figure 10. shows the PV module air-cooling thermal efficiency at different irradiances and ambient temperatures. Higher thermal efficiency was 53.5% for *G*=800 W and T_{am}=35℃ compared with a lower efficiency of 48% for *G*=1000 W and T_{am}=45℃. Thermal efficiency of the solar PV module air-cooling can be influenced by many parameters such as air flowrate, air thermophysical properties, temperature difference between inlet and outlet airflow in the cooling channel, and solar radiation intensity. Therefore, from the definition, the case at *G*=800 W and T_{am}=35℃ had revealed a greater ratio between the heat gain of the air flowing in the cooling duct and incident irradiance which enhance the thermal efficiency compared with other testing cases. The PV module electrical efficiency versus Reynold's number at different irradiances and T_{am}=45℃ is shown in Figure 11. A noticeable rise in a module efficiency with *Re* increasing can be seen for all irradiances 800, 900, and 1000 W. The drop in the PV module temperature depends on panel air cooling performance which based on a forced convection heat transfer and thus it significantly enhanced by *Re* increasing. The improvement in electrical efficiency of PV module with air-cooling was greater by about 4%, 4.4% and 5% for irradiances 800, 900 and 1000 W respectively compared to that without cooling as shown in Figure 11. Maximum module electrical efficiency was about 13.66% at *G*=800W compared to 13.6% and 13.52% for irradiances 900W and 1000W respectively. Therefore, improving the PV module cooling performance will enhance the module output power and electrical efficiency which leads to extending the solar PV module lifecycle.

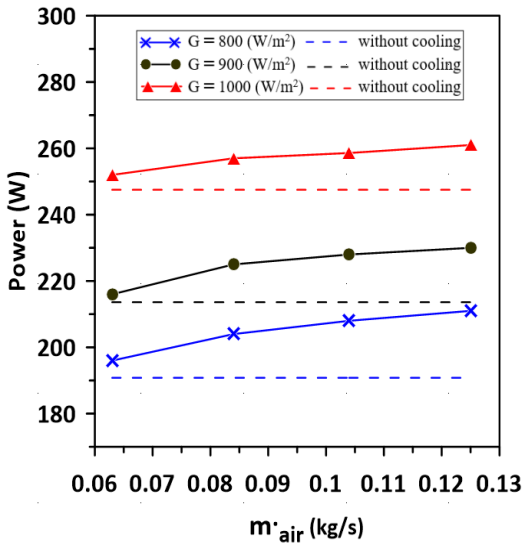

Figure 9. Variation of the PV module output power with air flowrate at different irradiances and T_{am}=45℃

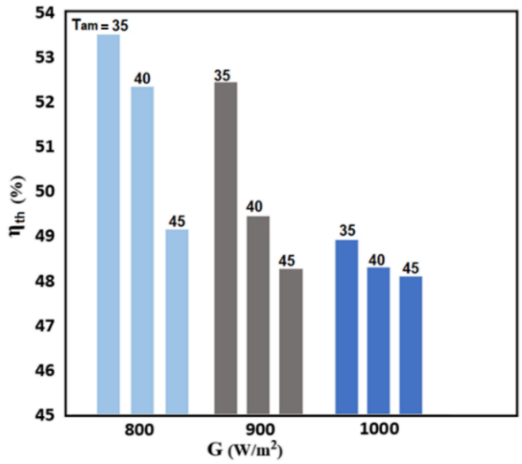

Figure 10. PV module cooling thermal efficiency at different irradiances and ambient temperatures for $\dot{m}_{air}$=0.084 kg/s

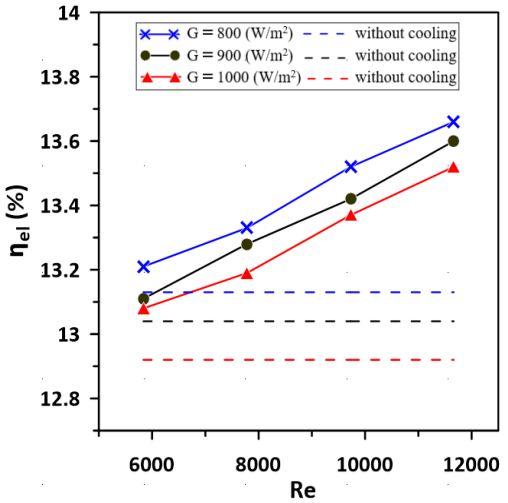

Figure 11. PV module electrical efficiency versus *Re* at different irradiances and T_{am}=45°C

3.2 Numerical results

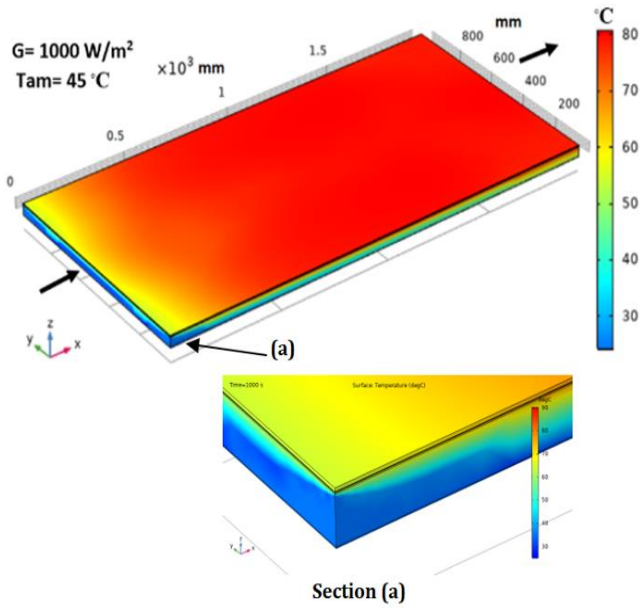

Figure 12. Temperature distribution in PV panel and cooling channel at T_{am}=45°C and G=1000 W/m²

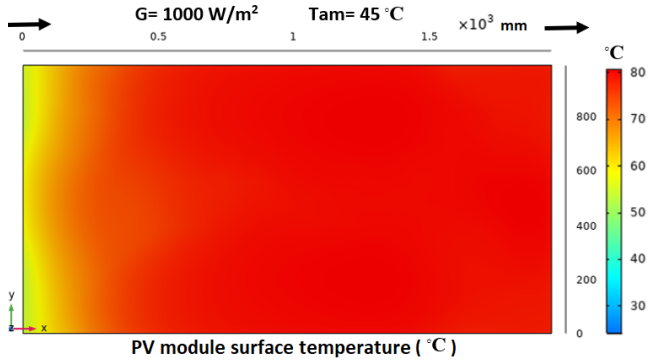

Figure 13. Temperature distribution along solar PV panel surface at T_{am}=45°C and G=1000 W/m²

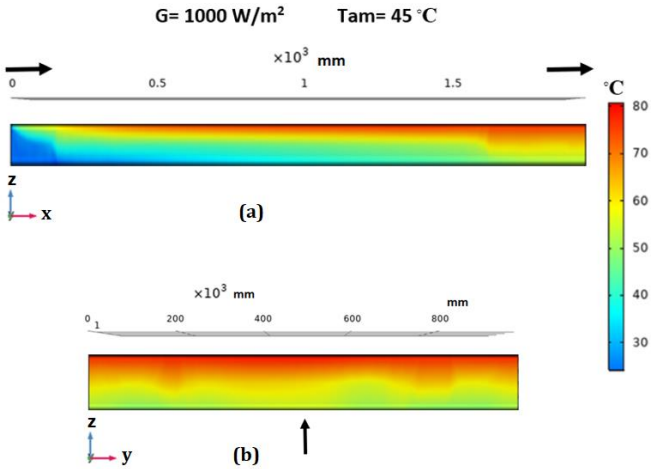

Figure 14. Temperature distribution along PV module cooling channel at T_{am}=45°C and G=1000 W/m²

The mathematical model of simulated PV module air-cooling system was solved numerically using COMSOL-5.4 software. Selected numerical results of the temperature distribution along PV module surface and cooling channel at relatively hot climatic conditions (T_{am}=45°C and G=1000 W/m²) are shown in Figures 12-15. Temperature distribution along PV panel and cooling channel is illustrated in Figure 12, where a higher temperature in the range of 70-78°C can be observed at middle and end regions of the solar PV panel. This trend in the temperature distribution can be attributed to the effect of air cooling which is varies between the inlet and outlet of the air channel. A lower PV panel temperature in the range of 60-65°C can be seen at cooling channel inlet due to the heat exchange increasing between the inlet air at relatively lower temperature and PV panel back surface. The air temperature in the cooling channel is varies from 45 to 60°C at channel inlet and outlet respectively as shown in this figure. A similar trend in the PV panel temperature distribution can be seen in Figure 13 along x-y direction of the panel surface. Figure 14 shows the temperature distribution along PV panel cooling channel at T_{am}=45°C and G=1000 W/m². A significant difference along x-z section of the cooling channel is observed due to the gradient in the air temperature between the inlet and outlet of the cooling channel which is reflects the effect of air cooling on PV panel along cooling channel as shown in Figure 14a. The variation in in the air temperature along y-z section of the cooling channel is shown in Figure 14b. The temperature was about 58°C for the air close the lower insulated surface and 70°C for the air close to the hot upper

channel surface which is attached with the PV panel subjected to the solar radiation. The variation in temperature distribution along cooling channel and PV panel is also depicted in Figure 15a and Figure 15b respectively which show the isotherm diagram for the PV module system at T_{am}=45°C and G=1000 W/m^2.

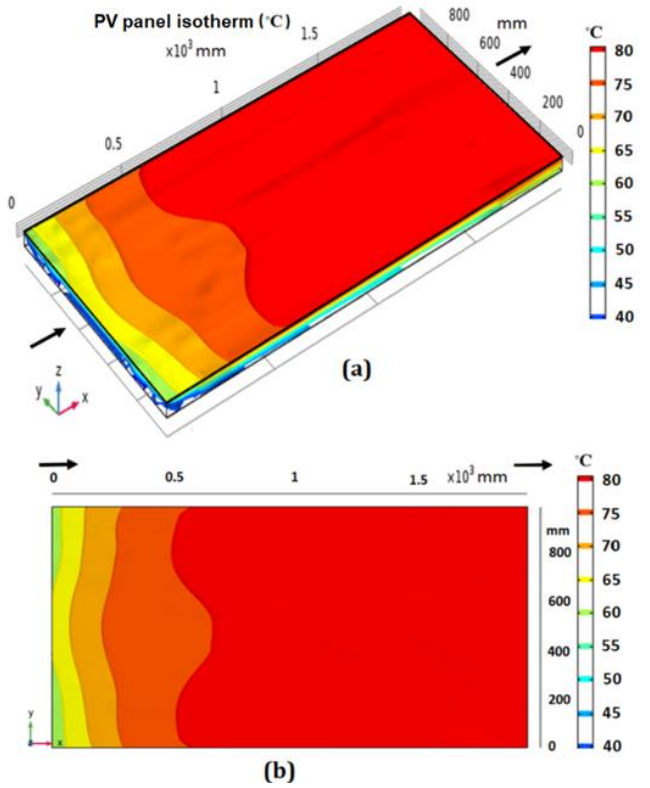

Figure 15. Solar PV panel isotherm diagram at T_{am}=45°C and G=1000 w/m^2: (a) PV panel with cooling channel, n x-z section; (b) PV panel surface, in y-z section

3.2.1 Validation of the numerical results

To investigate the accuracy of the numerical solution for PV module and cooling system simulation model, the numerical results were validated with the experimental results of the present study as shown in Figures 16-18. Comparison of the experimental and numerical PV panel temperature variation with *Re* at T_{am}=45°C is depicted in Figure 16. An average deviation of 9% can be observed between numerical and experimental results for irradiances 800, 900 and 1000 W due to the assumptions of the simulation model numerical solution and uncertainties of the experimental data. Figure 17 shows the comparison of the numerical PV module electrical efficiency with the experimental data at T_{am}=45°C and various irradiances. The numerical and experimental results follow a similar trend as shown in this figure with an average deviation of about 3.5% between them. The simulated module electrical efficiency was lower than that of the experimental data for all test cases. The reason for this deviation is attributed to a relatively higher simulated panel temperatures compared to the experimental date which resulted in a drop in the numerical electrical efficiency. Figure 18 shows the comparison of the experimental and numerical results of the PV module thermal efficiency at T_{am}=45°C and air flowrate of 0.084 kg/s. The numerical thermal efficiency of the PV module was greater than experimental results by about 3.8% at different irradiances. It can be concluded that the numerical solution has reflected an acceptance estimation of the module performance parameters compared to the experimental data. in a drop in the numerical module electrical efficiency.

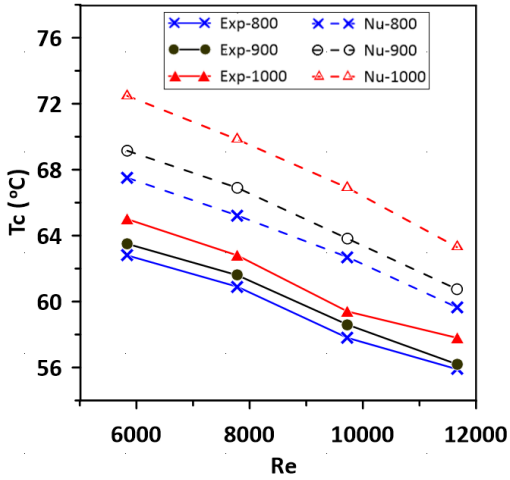

Figure 16. Comparison of the experimental and numerical results of the *Tc* variation with *Re* at T_{am}=45°C

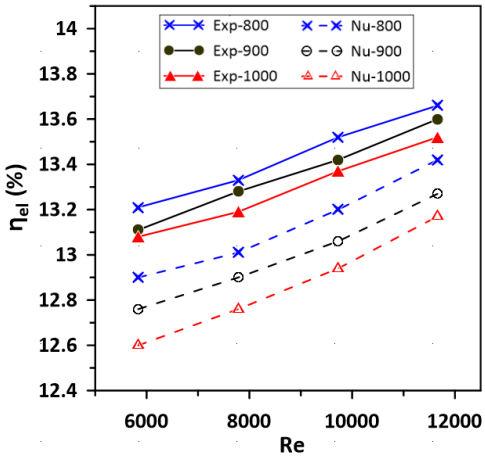

Figure 17. Comparison of the experimental and numerical results of the η_{el} at T_{am}=45°C

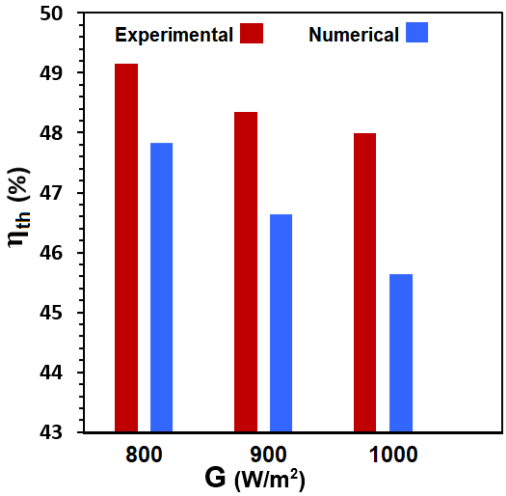

Figure 18. Comparison of the experimental and numerical results of η_{th} at T_{am}=45°C and $\dot{m}_{air}$=0.084 kg/s

3.3 Comparison with reported experimental data

The comparison of the present work results with the similar

reported works results Elbreki [21] and Arifin [23] are shown in the Figure 19 and Figure 20 respectively. Due to the difference in the testing conditions, the comparison was based on selected similar operating conditions at ambient temperature in the range of 32-35℃ and Reynold's number in the range of 5500-6000. Figure 19 shows the comparison of the present work results with results of Elbreki [21] and Arifin [23] for the solar PV panel temperature variation with irradiance. The difference in the results of the solar panel temperature without and with air cooling were about 12.7%, 31.8% and 19.7% for present study, Elbreki and Zainal works respectively. Comparison of the results for the solar PV module electrical efficiency is depicted in Figure 20. It can be seen a variation in the efficiency for the PV module without and with cooling by about 9%, 12% and 22% for present study, Elbreki and Arifin experimental data respectively. The compared results follow a similar trend in spite of some differences in the rating power and type of the PV module employed in the testing cases, in addition to some differences in the operating conditions.

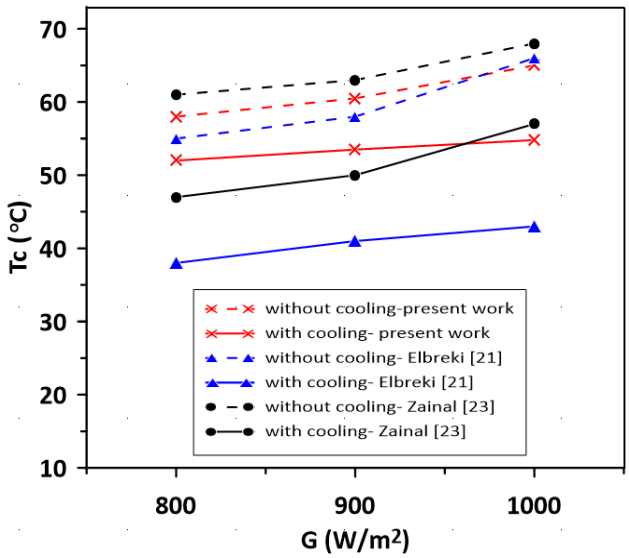

Figure 19. Comparison of the present results with reported experimental data [21, 23] at T_{am} in the range of 32-35℃

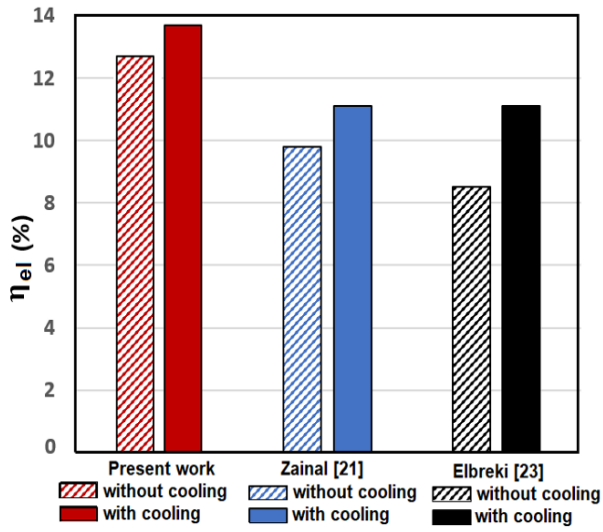

Figure 20. Comparison of the present results with reported experimental data [21, 23] for η_{el} at G=1000 W and T_{am} in the range of 32-35℃

4. CONCLUSION

The effect of air-cooling on solar PV module performance under hot climatic conditions was investigated experimentally and numerically based on different ambient temperatures 35, 40, 45℃ and irradiances 800, 900, 1000 W. The results revealed a noticeable drop in the PV panel temperature with cooling air flowrate increasing under different testing conditions. The maximum module temperature was about 65℃ at G=1000W, T_{am}=45℃ and relatively minimum air flowrate of 0.063 kg/s. The output power, electrical efficiency, and thermal efficiency for the PV module with air cooling reflected an improvement by about 8.2%, 7% and 5.4% for irradiances 800, 900 and 1000 W respectively compared to that without cooling. Higher thermal efficiency of the PV module air-cooling was 53.5% for G=800 W and T_{am}=35℃ compared with a lower efficiency of 48% for G=1000 W and T_{am}=45℃. The numerical and experimental results followed a similar trend with an average deviation of about 9%, 3.5% and 3.8% in PV module temperature, electrical efficiency and thermal efficiency respectively at T_{am}=45℃ and various irradiances.

ACKNOWLEDGMENT

The authors would like to thank the renewable energy center and workshop at the Engineering Technical College-Baghdad/ Middle Technical University for their support in fabricating the experimental test rig and providing the measurement devices.

REFERENCES

[1] Charles Lawrence Kamuyu, W., Lim, J.R., Won, C.S., Ahn, H.K. (2018). Prediction model of photovoltaic module temperature for power performance of floating PVs. Energies, 11(2): 447. https://doi.org/10.3390/en11020447

[2] Skoplaki, E.P.J.A., Palyvos, J.A. (2009). Operating temperature of photovoltaic modules: A survey of pertinent correlations. Renewable Energy, 34(1): 23-29. https://doi.org/10.1016/j.renene.2008.04.009

[3] Bayrakci, M., Choi, Y., Brownson, J.R. (2014). Temperature dependent power modeling of photovoltaics. Energy Procedia, 57: 745-754. https://doi.org/10.1016/j.egypro.2014.10.282

[4] Ubertini, S., Desideri, U. (2003). Performance estimation and experimental measurements of a photovoltaic roof. Renewable Energy, 28(12): 1833-1850. https://doi.org/10.1016/S0960-1481(03)00073-9

[5] Glick, A., Ali, N., Bossuyt, J., Calaf, M., Cal, R.B. (2020). Utility-scale solar PV performance enhancements through system-level modifications. Scientific reports, 10(1): 10505. https://doi.org/10.1038/s41598-020-66347-5

[6] Dubey, S., Sarvaiya, J.N., Seshadri, B. (2013). Temperature dependent photovoltaic (PV) efficiency and its effect on PV production in the world–a review. Energy Procedia, 33: 311-321. https://doi.org/10.1016/j.egypro.2013.05.072

[7] Sahin, G. (2018). Effect of temperature on the capacitance of a silicon solar cell in static regime. Energy

and Power Engineering, 10(5): 187-197. https://doi.org/10.4236/epe.2018.105013
[8] Al-Kouz, W., Al-Dahidi, S., Hammad, B., Al-Abed, M. (2019). Modeling and analysis framework for investigating the impact of dust and temperature on PV systems' performance and optimum cleaning frequency. Applied Sciences, 9(7): 1397. https://doi.org/10.3390/app9071397
[9] Chander, S., Purohit, A., Sharma, A., Nehra, S.P., Dhaka, M.S. (2015). A study on photovoltaic parameters of mono-crystalline silicon solar cell with cell temperature. Energy Reports, 1: 104-109. https://doi.org/10.1016/j.egyr.2015.03.004
[10] Bahaidarah, H., Rehman, S., Subhan, A., Gandhidasan, P., Baig, H. (2015). Performance evaluation of a PV module under climatic conditions of Dhahran, Saudi Arabia. Energy Exploration & Exploitation, 33(6): 909-929. https://doi.org/10.1260/0144-5987.33.6.909
[11] Sanusi, Y.K., Fajinmi, G.R., Babatunde, E.B. (2011). Effects of ambient temperature on the performance of a photovoltaic solar system in a tropical area. The Pacific Journal of Science and Technology, 12(2): 176-180.
[12] Hamad, A.J. (2020). Performance evaluation of polycrystalline photovoltaic module based on varying temperature for Baghdad city climate. Journal of Advanced Research in Fluid Mechanics and Thermal Sciences, 68(2): 164-176.
[13] Aoun, N. (2021). Outdoor testing of free standing PV module temperature under desert climate: A comparative study. International Journal of Ambient Energy, 42(13): 1484-1491. https://doi.org/10.1080/01430750.2019.1611640
[14] Sharaf, M., Yousef, M.S., Huzayyin, A.S. (2022). Review of cooling techniques used to enhance the efficiency of photovoltaic power systems. Environmental Science and Pollution Research, 29(18): 26131-26159. https://doi.org/10.1007/s11356-022-18719-9
[15] El Kharaz, H., Khallaki, K., Kadiri, M.S., Choukairy, K. (2021). Performance's improvement methods of PV solar panel by different cooling systems: A Review of Experimental and Numerical studies. In AIP Conference Proceedings, 2345(1): 020039. https://doi.org/10.1063/5.0049573
[16] Hasanuzzaman, M., Malek, A.B.M.A., Islam, M.M., Pandey, A.K., Rahim, N.A. (2016). Global advancement of cooling technologies for PV systems: A review. Solar Energy, 137: 25-45. http://dx.doi.org/10.1016/j.solener.2016.07.010
[17] Alkhalidi, A., Khawaja, M.K., Kelany, A., Ghaffar, A. (2019). Investigation of repurposed material utilization for environmental protection and reduction of overheat power losses in PV panels. International Journal of Photoenergy, 2019: 2181967. https://doi.org/10.1155/2019/2181967
[18] Bayrak, F., Oztop, H.F., Selimefendigil, F. (2019). Effects of different fin parameters on temperature and efficiency for cooling of photovoltaic panels under natural convection. Solar Energy, 188: 484-494. https://doi.org/10.1016/j.solener.2019.06.036
[19] Hasan, I.A., Attar, D.A. (2019). Effect of evaporative cooling combined with heat sink on PV module performance. Journal of University of Babylon for Engineering Sciences, 27(2): 252-264. https://doi.org/10.29196/jubes.v27i2.2345
[20] Egab, K., Okab, A., Dywan, H.S., Oudah, S.K. (2020). Enhancing a solar panel cooling system using an air heat sink with different fin configurations. In IOP Conference Series: Materials Science and Engineering, 671(1): 012133. https://doi.org/10.1088/1757-899X/671/1/012133
[21] Elbreki, A.M., Muftah, A.F., Sopian, K., Jarimi, H., Fazlizan, A., Ibrahim, A. (2021). Experimental and economic analysis of passive cooling PV module using fins and planar reflector. Case Studies in Thermal Engineering, 23: 100801. https://doi.org/10.1016/j.csite.2020.100801
[22] Dwivedi, P., Sudhakar, K., Soni, A., Solomin, E., Kirpichnikova, I. (2020). Advanced cooling techniques of PV modules: A state of art. Case Studies in Thermal Engineering, 21: 100674. https://doi.org/10.1016/j.csite.2020.100674
[23] Arifin, Z., Tjahjana, D.D.D.P., Hadi, S., Rachmanto, R.A., Setyohandoko, G., Sutanto, B. (2020). Numerical and experimental investigation of air cooling for photovoltaic panels using aluminum heat sinks. International Journal of Photoenergy, 2020: 1574274. https://doi.org/10.1155/2020/1574274
[24] Naghavi, M.S., Esmaeilzadeh, A., Singh, B., Ang, B.C., Yoon, T.M., Ong, K.S. (2021). Experimental and numerical assessments of underlying natural air movement on PV modules temperature. Solar Energy, 216: 610-622. https://doi.org/10.1016/j.solener.2021.01.007
[25] Asim, M., Milano, J., Khan, H.I., Hanzla Tahir, M., Mujtaba, M.A., Shamsuddin, A.H., Abdullah, M., Kalam, M.A. (2022). Investigation of mono-crystalline photovoltaic active cooling thermal system for hot climate of Pakistan. Sustainability, 14(16): 10228. https://doi.org/10.3390/su141610228
[26] Abed, A.F., Hachim, D.M., Najim, S.E. (2021). Numerical simulation of heat transfer from PV panel with a wetted porous wick. Basrah Journal for Engineering Sciences, 21(2): 29-38. http://dx.doi.org/10.33971/bjes.21.2.5
[27] Agyekum, E.B., PraveenKumar, S., Alwan, N.T., Velkin, V.I., Shcheklein, S.E. (2021). Effect of dual surface cooling of solar photovoltaic panel on the efficiency of the module: Experimental investigation. Heliyon, 7(9): e07920. https://doi.org/10.1016/j.heliyon.2021.e07920
[28] Alktranee, M., Bencs, P. (2022). Effect of evaporative cooling on photovoltaic module performance. Process Integration and Optimization for Sustainability, 6: 921-930. https://doi.org/10.1007/s41660-022-00268-w
[29] Zhang, Y., Shen, C., Zhang, C., Pu, J., Yang, Q., Sun, C. (2022). A novel porous channel to optimize the cooling performance of PV modules. Energy and Built Environment, 3(2): 210-225. https://doi.org/10.1016/j.enbenv.2021.01.003
[30] Jakhar, S., Soni, M.S., Gakkhar, N. (2017). Modelling and simulation of concentrating photovoltaic system with earth water heat exchanger cooling. Energy Procedia, 109: 78-85. https://doi.org/10.1016/j.egypro.2017.03.054
[31] Hattam, S.Y. (2022). Experimental and numerical study to improve the performance of solar cell using water cooling system. MSc. Thesis, Al-furat Al-awsat Technical University Engineering Technical College:

Najaf, Iraq.
[32] Zubeer, S.A., Ali, O.M. (2022). Experimental and numerical study of low concentration and water-cooling effect on PV module performance. Case Studies in Thermal Engineering, 34: 102007. https://doi.org/10.1016/j.csite.2022.102007
[33] Darwish, M., Moukalled, F. (2016). The finite volume method in computational fluid dynamics: An advanced introduction with OpenFOAM® and Matlab®. Springer International Publishing Switzerland, FMIA.
[34] Versteeg, H.K., Malalasekera, W. (2007). An Introduction to Computational Fluid Dynamics. Pearson Education Limited, second edition.
[35] Lamaamar, I., Tilioua, A., Alaoui, M.A.H. (2022). Thermal performance analysis of a poly c-Si PV module under semi-arid conditions. Materials Science for Energy Technologies, 5: 243-251. https://doi.org/10.1016/j.mset.2022.03.001
[36] Aneli, S., Arena, R., Gagliano, A. (2021). Numerical simulations of a PV module with phase change material (PV-PCM) under variable weather conditions. International Journal of Heat and Technology, 39(2): 643-652. https://doi.org/10.18280/ijht.390236
[37] Islam, M.N., Assaduzzaman, K., Hoq, M. (2012). Study and analysis of energy conversion using solar cell. International Journal of Electrical and Power Engineering, 6(1): 26-31. https://doi.org/10.3923/ijepe.2012.26.31
[38] Tiwari, G.N., Swapnil D. (2010). Fundamentals of Photovoltaic Modules and Their Applications. No. 2. Royal Society of Chemistry.

NOMENCLATURE

A_c	Air channel cross sectional area, (m^2)
Cp	Air specific heat, (J/kg. ℃)
D_h	Hydraulic diameter of the rectangular air channel, (m)
G	Solar radiation (irradiance), (W/m^2)
I_{mp}	Current at maximum output power, (Ampere)
K	Air thermal conductivity, (W/m. ℃)
m_{air}	Air mass flowrate, (kg/s)
Nu	Nusselt number, (-)
p	Rectangular air channel perimeter, (m)
P_c	Maximum output power of the solar PV module, (W)
Re	Reynold number, (-)
T_c	Temperature of the PV module surface, (℃)
T_i	Temperature of the channel inlet air flow, (℃)
T_m	Mean temperature of the air in the cooling channel, (℃)
T_o	Temperature of the channel outlet air flow, (℃)
v	Air flow velocity in the cooling channel, (m/s)
V_{mp}	Voltage at maximum output power, (Volt)

Greek symbols

α	Convection heat transfer coefficient, (W/m^2. ℃)
ρ	Air density, (kg/m^3)
η_{th}	Thermal efficiency of the PV module cooling, (%)
η_{el}	PV module electrical efficiency, (%)
η_{rf}	Reference efficiency of the PV module, (%)